

# PhysGM: Large Physical Gaussian Model for Feed-Forward 4D Synthesis

Chunji Lv<sup>1</sup>, Zequn Chen<sup>2</sup><sup>†</sup>, Donglin Di<sup>2</sup>, Weinan Zhang<sup>3</sup>, Hao Li<sup>2</sup>, Wei Chen<sup>2</sup>, Changsheng Li<sup>1</sup><sup>‡</sup>

Beijing Institute of Technology<sup>1</sup>, Li Auto Inc.<sup>2</sup>, Harbin Institute of Technology<sup>3</sup>

## Abstract

While physics-grounded 3D motion synthesis has seen significant progress, current methods face critical limitations. They typically rely on pre-reconstructed 3D Gaussian Splatting (3DGS) representations, while physics integration depends on either inflexible, manually defined physical attributes or unstable, optimization-heavy guidance from video models. To overcome these challenges, we introduce **PhysGM**, a feed-forward framework that jointly predicts a 3D Gaussian representation and its physical properties from a single image, enabling immediate, physical simulation and high-fidelity 4D rendering. We first establish a base model by jointly optimizing for Gaussian reconstruction and probabilistic physics prediction. The model is then refined with physically plausible reference videos to enhance both rendering fidelity and physics prediction accuracy. We adopt the Direct Preference Optimization (DPO) to align its simulations with reference videos, circumventing Score Distillation Sampling (SDS) optimization which needs back-propagating gradients through the complex differentiable simulation and rasterization. To facilitate the training, we introduce a new dataset PhysAssets of over 24,000 3D assets, annotated with physical properties and corresponding guiding videos. Experimental results demonstrate that our method effectively generates high-fidelity 4D simulations from a single image in one minute. This represents a significant speedup over prior works while delivering realistic rendering results. Our project page is at: <https://hihixiaolv.github.io/PhysGM.github.io/>

## Introduction

Recent advances in 3D representation, particularly 3D Gaussian Splatting (3DGS) (Kerbl et al. 2023), have revolutionized novel-view synthesis for static scenes. The next frontier is to imbue these representations with dynamic, physically plausible behavior, unlocking applications in virtual reality, robotics (Lu et al. 2024), and autonomous systems (Zhou et al. 2024). However, creating high-fidelity, physics-based 4D content remains a significant challenge, often demanding computationally expensive, per-scene optimization pipelines that are ill-suited for real-time or large-scale deployment.

Current paradigms for physics-based 4D synthesis are hampered by a fundamental bottleneck: a reliance on slow, iterative optimization. The typical workflow involves first reconstructing a 3DGS model from dense multi-view images,

then manually specifying its physical properties (e.g., stiffness, mass) via configuration files (Xie et al. 2024), and finally running a physics simulation. This process is not only computationally prohibitive but also lacks scalability and generalization. While recent works have explored learning physical properties by distilling knowledge from video models (Lin et al. 2025; Zhang et al. 2024c), these methods still require extensive per-scene training and fail to address the core issue of efficiency.

To overcome these limitations, we ask a fundamental question: Can we bypass per-scene optimization entirely and instead learn a generative model that produces a complete, physically-grounded 4D simulation in a single, feed-forward pass? This requires reframing the problem from one of slow, iterative reconstruction to one of amortized, feed-forward inference. To this end, we introduce **PhysGM**, a physics-grounded generative model that enables optimization-free synthesis of dynamic 4D scenes from sparse image inputs. Our key insight is a novel two-stage training paradigm designed to learn a generalizable physical prior and for perceptual realism. In the first stage, we pre-train our model on a substantial dataset to jointly predict a 3D Gaussian representation and its corresponding physical properties. This establishes a robust generative prior. In the second stage, we employ Direct Preference Optimization (DPO) (Rafailov et al. 2023) to fine-tune the model. By ranking generated simulations against a ground-truth video, we create preference pairs that guide the model towards producing more physically plausible and temporally coherent dynamic sequences, all without requiring a differentiable physics engine.

To facilitate this research, we construct and release the PhysAssets Dataset, a substantial benchmark of over 24,000 3D assets, each annotated with its physical material properties and a corresponding physically-plausible simulation video, providing a critical resource for training and evaluating generative 4D models.

Our main contributions are summarized as follows:

- We introduce PhysGM, the first feed-forward framework capable of generating a complete, physically-grounded 4D Gaussian simulation from sparse image inputs in under a minute.
- We propose a novel two-stage training paradigm that combines large-scale supervised pre-training with DPO-based refinement, enabling the model to learn a robust

<sup>†</sup> Project Leader. <sup>‡</sup> Corresponding Author.

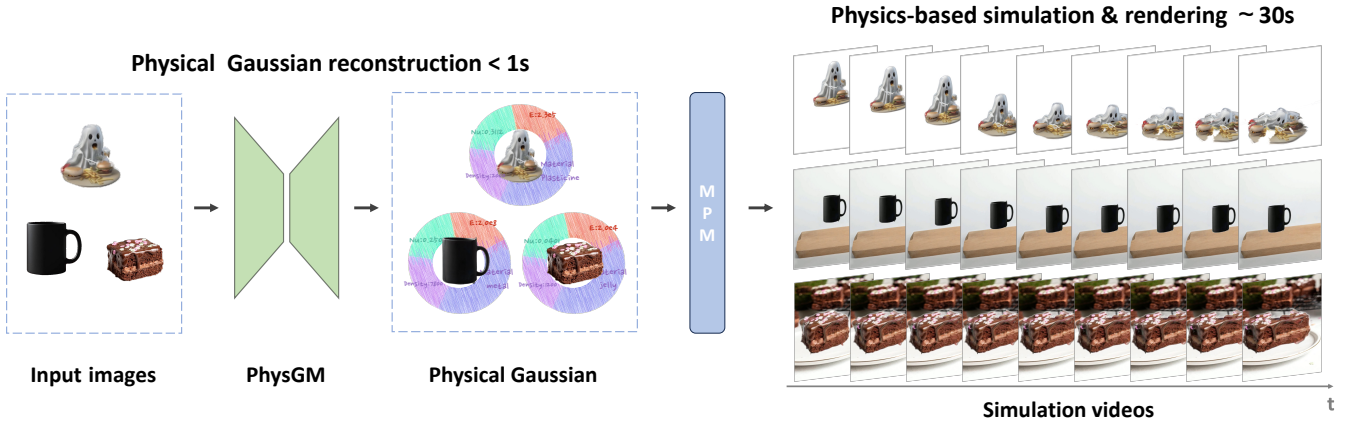


Figure 1: Overview of **PhysGM**. Given a single image, **PhysGM** performs a single feed-forward pass to directly predict 3D Gaussian Splatting (3DGS) representation and its associated physical properties (e.g., stiffness, mass). This prediction is optimization-free and completes in under one second. The generated parameters then initialize a Material Point Method (MPM) simulator, producing the final, physically plausible 4D animation.

physical prior and then align it with perceptual quality.

- We present the PhysAssets Dataset, a new substantial benchmark with 24,000+ assets annotated with physical properties and simulation videos, to spur future research in this domain.

## Related Work

### 4D Content Generation

The generation of 4D content—dynamic 3D scenes with temporal evolution—has recently seen rapid progress, largely branching into two main paradigms: distillation from 2D generative models and direct supervision on 3D data.

The first paradigm leverages powerful pre-trained 2D or video diffusion models as priors, using Score Distillation Sampling (SDS) (Poole et al. 2022) to optimize a dynamic 3D representation (Yin et al. 2023; Ren et al. 2023; Bahmani et al. 2024; Ling et al. 2024). Some approaches explicitly model temporal deformations, for instance, by using warped Gaussian surfaces (Wang et al. 2023a). To improve temporal consistency, other works employ multi-view video models for more robust supervision (Zhang et al. 2024a; Jiang et al. 2024). However, the iterative nature of SDS is computationally expensive and can be unstable. To mitigate this, some methods pre-synthesize full video sequences to use as direct supervision (Ren et al. 2023; Pan et al. 2024), while others propose generalizable models to bypass per-scene optimization entirely (Ren et al. 2024). The second paradigm trains generative models directly on paired text-3D data (Jun and Nichol 2023; Nichol et al. 2022). Pioneering works like Point-E (Nichol et al. 2022) generated point clouds, while more recent models like Shap-E (Jun and Nichol 2023) and LGM (Tang et al. 2024) produce implicit functions (SDFs) (Park et al. 2019) and explicit 3DGS representations (Kerbl et al. 2023), respectively. The primary drawback of this approach is its reliance on large-scale 3D datasets, which remain scarce.

Despite their visual progress, these methods are fundamentally agnostic to the laws of physics. Their focus on vi-

sual plausibility often yields animations that are temporally coherent but physically impossible, as they lack an explicit model of real-world dynamics.

### Feed-forward 3D Gaussian Models

Parallel to 4D generation, another line of research has focused on accelerating the creation of static 3D scenes. Traditional 3DGS reconstruction (Kerbl et al. 2023) requires slow, per-scene optimization. To address this, feed-forward models have emerged to perform 3D reconstruction from sparse or even single views in a single pass (Szymanowicz, Rupprecht, and Vedaldi 2024; Tang et al. 2024; Xu et al. 2024; Zhang et al. 2024b; Wu et al. 2024). Models like Splatter Image (Szymanowicz, Rupprecht, and Vedaldi 2024) and LGM (Tang et al. 2024) use U-Net-based architectures to directly regress Gaussian parameters from input images. Other works focus on scene-level generation by aggregating features from multiple images (Charatan et al. 2024; Chen et al. 2024; Hong et al. 2023; Li et al. 2023; Wang et al. 2023b).

However, these feed-forward models have been exclusively developed for static scene generation. They lack any mechanism to represent or predict dynamic, physics-based behavior, limiting their use to non-interactive applications. Our work is the first to embed physical reasoning directly into a feed-forward Gaussian generation framework.

### Physics-Grounded 4D Synthesis

The integration of physics into 4D generation is a nascent but critical field. The pioneering work, PhysGaussian (Xie et al. 2024), first coupled 3DGS with continuum mechanics simulation via the Material Point Method (MPM) in the Warp framework (Macklin 2022). This established a foundational pipeline but required expert-driven, manual configuration of physical parameters for each scene.

Subsequent research has focused on automating this parameterization. One popular approach uses SDS to distill motion priors from video models, enabling data-driven optimization of material properties (Zhang et al. 2024c; Huang

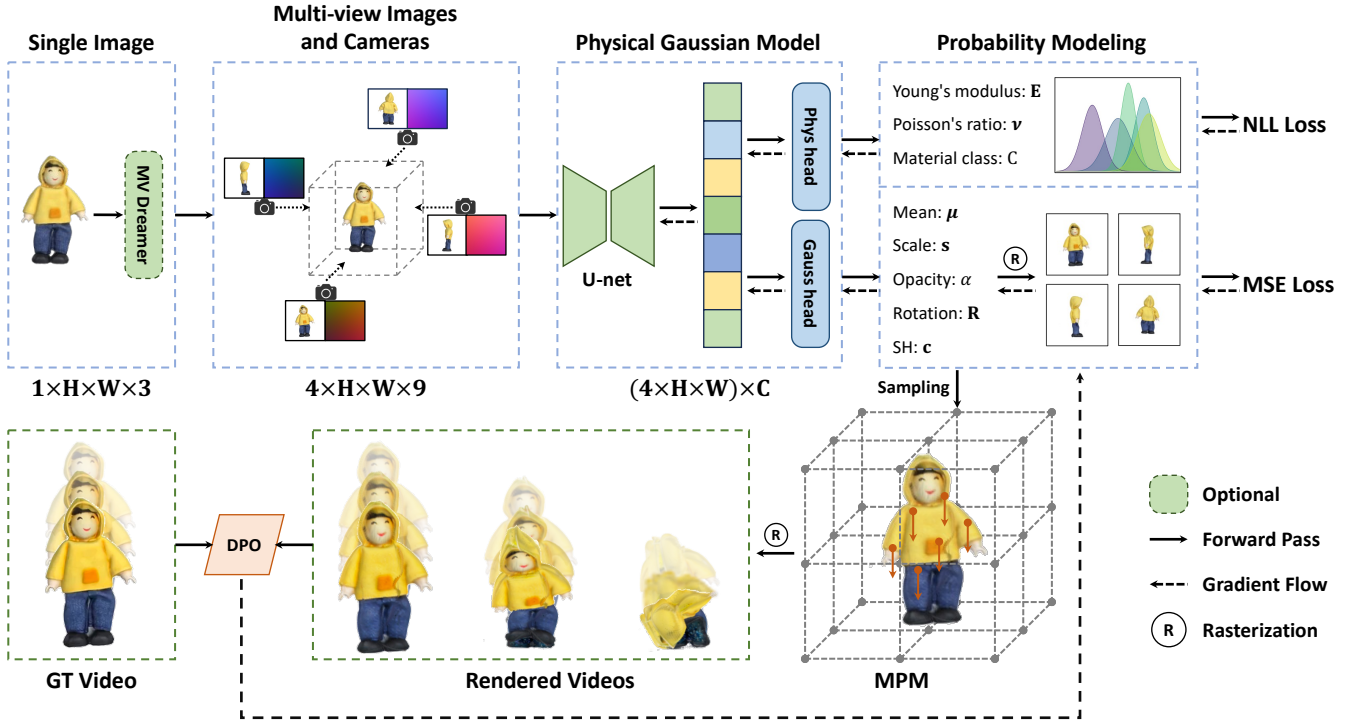


Figure 2: Architecture of **PhysGM**. The model conditions on one or more input views and their corresponding camera parameters, which are processed by a U-Net encoder to produce a shared latent representation  $\mathbf{z}$ . This latent is then decoded by two parallel heads: (1) a *Gaussian Head* predicting the initial 3D Gaussian scene parameters  $\psi$ , and (2) a *Physics Head* that predicts a distribution over the object’s physical properties  $\theta$ . The sampled parameters  $(\psi, \theta)$  initialize a Material Point Method (MPM) simulator to generate the final dynamic sequence. The entire architecture is trained in a two-stage paradigm: first, supervised pre-training on ground-truth data establishes a robust generative prior. Subsequently, a DPO-based fine-tuning stage uses the ranks against a ground-truth video and aligns the model with physically plausible results.

et al. 2025; Liu et al. 2024a; Tan et al. 2024). For instance, DreamPhysics (Huang et al. 2025) proposed a feature-disentanglement framework to separate motion and appearance. Others have explored using Large Language Models (LLMs) to infer parameters from text descriptions (Zhao et al. 2024; Chen et al. 2025; Liu et al. 2024b; Cai et al. 2024), though these can struggle with continuous physical quantities. More advanced methods learn neural constitutive models to represent complex material behaviors (Lin et al. 2025). Concurrently, efforts have been made to construct dedicated physical 3D datasets (Cao et al. 2025).

Despite these advances, the entire field suffers from two critical bottlenecks. First, these methods presuppose the existence of a high-quality, pre-optimized 3DGS model, requiring dense multi-view inputs and significant offline processing. Second, the process of imbuing this static model with physics is treated as a separate, per-scene optimization problem. This iterative fine-tuning, often taking hours to converge for a single object, renders existing approaches impractical for scalable content creation or any application requiring rapid generation. Our work, PhysGM, directly addresses these gaps. By integrating a feed-forward generative architecture with a learned physical prior, we eliminate the need for both per-scene optimization and pre-reconstructed 3D models. Our two-stage training paradigm allows us to produce physically grounded 4D simulations from sparse in-

puts at a speed several orders of magnitude faster than existing methods, bridging the gap between efficient generation and physical realism.

## Method

Given a single RGB image  $I \in \mathbb{R}^{H \times W \times 3}$ , our objective is to infer a physically-enabled 3D representation of the depicted object. This representation consists of two key components: (1) a set of 3D Gaussians,  $\psi = \{g_i\}_{i=1}^N$  that defines the object’s geometry and appearance, and (2) a corresponding vector of physical properties  $\theta$ . Formally, we aim to learn a feed-forward mapping function  $F$  such that:  $F(I) = (\psi, \theta)$ . This direct inference approach is designed to circumvent two critical bottlenecks in prior work: the need for slow, per-scene optimization to determine  $\psi$ , and the reliance on either manually defined physical priors  $\theta_{\text{manual}}$  or unstable, heavy optimization to estimate  $\theta$  from SDS loss. Our goal is to make both  $\psi$  and  $\theta$  predictable in a single feed-forward pass, enabling immediate, physics-based simulation. An overview of our pipeline is illustrated in Figure 2.

## 3D Gaussian Splatting

The core of 3DGS (Kerbl et al. 2023) is to model the scene as a set of  $N$  anisotropic 3D Gaussians. Each Gaussian is parameterized by: position  $\mu \in \mathbb{R}^3$ , defining its center in

world space; covariance  $\Sigma \in \mathbb{R}^{3 \times 3}$  defining its shape and orientation; opacity  $\alpha \in [0, 1]$  controlling its transparency; color represented by Spherical Harmonics (SH) coefficients  $\mathbf{c}$  to model view-dependent effects. The covariance matrix can be computed with a rotation matrix  $\mathbf{R}$  and a diagonal scaling matrix  $\mathbf{S}$ :  $\Sigma = \mathbf{RSS}^T\mathbf{R}^T$

During rendering, these 3D Gaussians are projected onto the 2D image plane for a given camera view. The final color  $\mathbf{C}$  for a pixel is computed by alpha-blending the  $N$  Gaussians that overlap the pixel:

$$\mathbf{C} = \sum_{i=1}^N \mathbf{c}'_i \alpha'_i \prod_{j=1}^{i-1} (1 - \alpha'_j), \quad (1)$$

where  $\mathbf{c}'_i$  is the view-dependent color evaluated from the SH coefficients, and  $\alpha'_i$  is the effective opacity of the  $i$ -th Gaussian. The objective of all parameters  $\psi = \{(\mu_i, \mathbf{q}_i, \mathbf{s}_i, \alpha_i, \mathbf{c}_i)\}_{i=1}^N$  is to minimize the difference between the rendered and ground-truth images.

### Probabilistic Modeling

To infer the physical and appearance parameters of an object, we first derive a 3D-aware latent representation  $\mathbf{z}$  from the single input image  $I$ . This is achieved in two steps. First, we use MVDream (Shi et al. 2023) to generate four consistent novel views from the input image. Second, a U-Net encoder fuses these views and their associated camera embeddings into the latent vector  $\mathbf{z}$ . This vector then conditions the subsequent prediction of physical properties and dynamic appearance parameters.

**Probabilistic Physics Modeling** We focus on three key physical attributes that govern the behavior of deformable objects: a material class  $C$ , Young’s modulus  $E$  (stiffness), Poisson’s ratio  $\nu$  (compressibility) and density  $\rho$ . We categorize materials into  $N_c$  discrete classes, where each class corresponds to a specific constitutive model used in the subsequent MPM simulation.

From the latent feature vector  $\mathbf{z}$ , we predict these properties using two specialized heads: A classification head  $f_{\text{material}}$  to determine the material class; A multi-layer perceptron (MLP) head,  $f_{\text{phys}}$  predicting the normal distribution for the continuous physical properties  $\theta = [E, \nu, \rho]^T$ . Specifically,  $f_{\text{phys}}$  outputs the mean  $\mu_\theta$  and log-variance  $\log \sigma_\theta^2$  for these properties:

$$(\mu_\theta, \log \sigma_\theta^2) = f_{\text{phys}}(\mathbf{z}). \quad (2)$$

This defines a conditional probability distribution over the physical properties, allowing us to model the inherent uncertainty in estimating physics from visual data:

$$P(\theta|I) = \mathcal{N}(\theta|\mu_\theta, \text{diag}(\sigma_\theta^2)). \quad (3)$$

**Probabilistic Appearance Modeling** For each of the  $N$  Gaussians comprising the scene, we predict a full set of its defining parameters, denoted as  $\psi$ . Similar to Section , a dedicated network head  $f_{\text{gauss}}$  processes the latent feature vector  $\mathbf{z}$  to output the parameters of a Gaussian distribution for the scene’s attributes:

$$(\mu_\psi, \log \sigma_\psi^2) = f_{\text{gauss}}(\mathbf{z}). \quad (4)$$

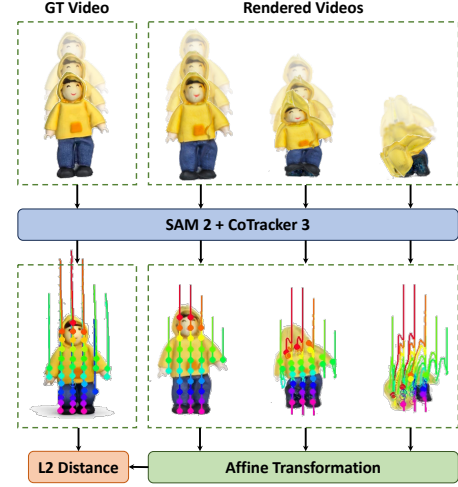


Figure 3: Preference calculation. We use SAM-2 for instance segmentation and CoTracker-3 for trajectory extraction across the GT and simulated videos. The extracted point tracks quantify the fidelity of each candidate to the GT, yielding a ranked preference tuple.

This defines the conditional probability of the full set of Gaussian parameters given the initial image:

$$P(\psi|I) = \mathcal{N}(\psi|\mu_\psi, \text{diag}(\sigma_\psi^2)). \quad (5)$$

During pre-training, the network is optimized via a dual objective. It jointly minimizes the Negative Log-Likelihood (NLL) of the ground-truth physical and geometric parameters under the model’s predicted distributions, and a photometric reconstruction loss between the image rendered from the generated Gaussians and the ground-truth view. This joint supervision ensures that the learned generative prior is not only physically accurate but also capable of producing high-quality scene representations.

At inference time, we sample from these learned distributions to obtain a specific instance of the scene’s parameters:  $\psi_{\text{sampled}} \sim P(\psi|\mathbf{z})$ ,  $\theta_{\text{sampled}} \sim P(\theta|\mathbf{z})$ . This probabilistic formulation is crucial, as it allows the model to generate diverse Gaussian and physical parameters, enabling the subsequent preference-based refinement with GT videos.

### Physics-based Dynamics via MPM

To simulate physically based dynamics, we employ the Material Point Method (MPM) (Jiang et al. 2016; Stomakhin et al. 2013), a hybrid Lagrangian-Eulerian approach that discretizes an object into a set of material points. Each point  $p$  carries its own physical state, including mass  $m_p$ , position  $\mathbf{x}_p$ , velocity  $\mathbf{v}_p$ , and the affine velocity matrix  $\mathbf{C}_p$ . Crucially, it also tracks the deformation gradient  $\mathbf{F}_p$ , which maps vectors from the material’s rest configuration to its current deformed state.

The simulation evolves these states through a two-step process at each time step  $\Delta t$ . First, in the Particle-to-Grid (P2G) transfer, particle properties are mapped to a background Eulerian grid. The mass  $m_i$  and momentum  $\mathbf{p}_i$  at



Image	Simulated & Rendered videos	Predicted Physical Property
		Material : "Ceramics" E : 2.0e7    nu : 0.2637
		Material : "Jelly" E : 2.0e4    nu : 0.2434
		Material : "Stone" E : 2.0e7    nu : 0.1547
		Material : "Plasticine" E : 2.3e5    nu : 0.3112
		Material : "Snow" E : 8.0e4    nu : 0.2579

Figure 4: Qualitative results by **PhysGM**. For different objects, we show the single input image (left), keyframes from the resulting physically-plausible simulation (middle), and the physical properties predicted by our model (right). Our method generates these high-fidelity 4D sequences in under one minute from a single view, without any per-scene optimization.

each grid node  $i$  are computed via weighted summation:

$$m_i = \sum_p m_p N(\mathbf{x}_i - \mathbf{x}_p), \quad (6)$$

$$\mathbf{p}_i = \sum_p m_p (\mathbf{v}_p + \mathbf{C}_p(\mathbf{x}_i - \mathbf{x}_p)) N(\mathbf{x}_i - \mathbf{x}_p), \quad (7)$$

where  $N(\cdot)$  is a B-spline interpolation kernel. On the grid, internal forces (derived from  $\mathbf{F}_p$  and a constitutive model) and external forces (e.g., gravity) are computed and used to update grid velocities.

Second, in the Grid-to-Particle (G2P) transfer, the updated grid velocity field is interpolated back to update the particle states. The particle’s velocity and deformation gradient are updated as follows:

$$\mathbf{v}_p^{n+1} = \sum_i \frac{\mathbf{p}_i^{n+1}}{m_i} N(\mathbf{x}_i - \mathbf{x}_p), \quad (8)$$

$$\mathbf{F}_p^{n+1} = \left( \mathbf{I} + \Delta t \sum_i \frac{\mathbf{p}_i^{n+1}}{m_i} \nabla N(\mathbf{x}_i - \mathbf{x}_p)^T \right) \mathbf{F}_p^n. \quad (9)$$

The particle’s final position is  $\mathbf{x}_p^{n+1} = \mathbf{x}_p^n + \Delta t \mathbf{v}_p^{n+1}$ .

Following PhysGaussian (Xie et al. 2024), we directly couple this physical simulation with our 3D Gaussian representation. We establish a one-to-one correspondence between each material point and a Gaussian primitive. The updated particle position  $\mathbf{x}_p$  directly defines the Gaussian’s mean  $\boldsymbol{\mu}$ . More importantly, the deformation gradient  $\mathbf{F}_p$  dictates the Gaussian’s anisotropic shape and orientation. We perform a polar decomposition on  $\mathbf{F}_p$  to factor it into a

rotation matrix  $\mathbf{R}_p$  and a symmetric positive semi-definite stretch tensor  $\mathbf{S}_p$ ,  $\mathbf{F}_p = \mathbf{R}_p \mathbf{S}_p$ . The resulting rotation  $\mathbf{R}_p$  and the diagonal elements of the stretch tensor  $\mathbf{S}_p$  are then used to define the Gaussian’s rotation matrix  $\mathbf{R}$  and scaling vector  $\mathbf{s}$ , respectively. These are then used to construct the covariance matrix  $\boldsymbol{\Sigma}$ , thus ensuring the rendered geometry precisely mirrors the physically simulated deformation.

### Preference-based Fine-tuning with DPO

While supervised pre-training provides a robust physical prior, it may not fully capture the subtle dynamics that lead to high perceptual quality. To bridge this gap, we introduce a fine-tuning stage using Direct Preference Optimization (DPO) (Rafailov et al. 2023). This approach allows us to refine our generative model using feedback from the full physics simulation and rendering pipeline without requiring this pipeline to be differentiable.

We treat the pre-trained model as a fixed reference policy,  $\pi_{\text{ref}}$ . The model being optimized,  $\pi_\omega$ , is then refined using a dataset of preference pairs  $\mathcal{D} = \{(\mathbf{z}, \phi_w, \phi_l)\}$ . For each scene context  $\mathbf{z}$ , we perform the following steps to create a preference pair. First, we draw a set of  $K$  candidate parameter vectors  $\{\phi_1, \dots, \phi_K\}$  from our current policy, where  $\phi_k \sim \pi_\omega(\cdot | \mathbf{z})$ . Each  $\phi$  consists of the predicted physical properties  $\theta$  and appearance parameters  $\psi$ . For each candidate  $\phi_k$ , we run the MPM simulation and render the resulting 3D Gaussian sequence to produce a short video clip  $V_k$ . We compare each generated clip  $V_k$  to the ground-truth video  $V_{gt}$  using a perceptual distance metric  $d(V_k, V_{gt})$ . The parameter set  $\phi_k$  that yields the lowest perceptual distance is

Gen-Video		"An object made of stone falls down onto the invisible ground."
w/o DPO		Material : "Stone" E : 2.0e4    nu : 0.2212
w/ DPO		Material : "Stone" E : 2.0e7    nu : 0.1547
Gen-Video		"An object made of metal falls down onto the invisible ground."
w/o DPO		Material : "Metal" E : 2.0e4    nu : 0.2108
w/ DPO		Material : "Metal" E : 3.3e6    nu : 0.2563

Figure 5: Ablation results of DPO: The results indicate that after the two-stage DPO training, the model predicts physical attributes with greater accuracy, enabling the generation of 4D videos that exhibit higher physical fidelity.

designated the “winner”  $\phi_w$ . Another sample with a higher distance is chosen as the “loser”  $\phi_l$ .

These dynamically generated preference pairs are used to fine-tune  $\pi_\omega$  by minimizing the DPO loss. This objective directly increases the likelihood of the model generating the “winner” parameters while decreasing the likelihood of the “loser” parameters, relative to the reference policy:

$$L_{\text{DPO}}(\pi_\omega, \pi_{\text{ref}}) = -\mathbb{E}_{(\mathbf{z}, p_w, p_l) \sim D} [\log \sigma(p_1 - p_2)], \quad (10)$$

$$p_1 = \beta \log \frac{\pi_\omega(p_w | \mathbf{z})}{\pi_{\text{ref}}(p_w | \mathbf{z})}, \quad p_2 = \beta \log \frac{\pi_\omega(p_l | \mathbf{z})}{\pi_{\text{ref}}(p_l | \mathbf{z})}, \quad (11)$$

where  $\beta$  is a temperature parameter controlling the optimization strength. By optimizing this objective, we effectively steer the learned distribution towards regions of the parameter space that produce perceptually and physically superior simulations, without the need for optimization upon complex differentiable MPM and rendering process.

### PhysAssets Dataset

We introduce PhysAssets, a multi-modal dataset of over 24,000 3D objects designed to establish a robust mapping between object geometry and physical properties. The 3D assets were aggregated from established datasets, including Objaverse (Deitke et al. 2023), OmniObject3D (Wu et al. 2023), ABO (Collins et al. 2022), and GSO (Downs et al. 2022). To annotate physical attributes, we developed a pipeline leveraging a Vision-Language Model (VLM) SigLIP-2 (Tschannen et al. 2025). For each object, we compute the cross-modal similarity between multi-view images and predefined textual descriptors for material properties. The ground-truth (GT) video is generated for each object using the FramePack model (Zhang and Agrawala 2025) with text instructions on the detailed description of the physical properties of the object. We automate preference labeling

$d(V_k, V_{gt})$  via a comparative analysis pipeline, as shown in Figure 3. This involves using SAM-2 (Kirillov et al. 2023; Ravi et al. 2024) for instance segmentation and CoTracker-3 (Karaev et al. 2024b,a) for trajectory extraction across the GT and simulated videos. The extracted point tracks then quantify the fidelity of each candidate relative to the GT, yielding a ranked preference tuple. More details on video generation and preference calculation process can be found in supplementary materials.

## Experiments

In this section, we conduct a comprehensive comparison against several baseline methods, evaluating the stability of fine-grained physical properties. Furthermore, we perform ablation studies on our two-stage training strategy to validate its effectiveness.

### Experimental settings

**Dataset** We train and evaluate our model on our newly created PhysAssets Dataset. For qualitative visualizations, we show results on the test set from our dataset as well as on in-the-wild images to demonstrate generalization.

**Baselines** We compare our method against two baseline models in physics-based dynamic generation: OmniPhysGS (Lin et al. 2025) and DreamerPhysics (Huang et al. 2025). These methods represent the dominant paradigm of per-scene optimization, where physical properties are learned by distilling knowledge from video models using Score Distillation Sampling (SDS). They provide strong benchmarks for simulation quality, albeit at a significant computational cost.

**Simulation Process** The physical properties predicted by our model directly drive the subsequent Material Point

Method	metal		jelly		plasticine		snow		sand		average	
	CLIP <sub>sim</sub>	UPR	CLIP <sub>sim</sub>	UPR	CLIP <sub>sim</sub>	UPR	CLIP <sub>sim</sub>	UPR	CLIP <sub>sim</sub>	UPR	CLIP <sub>sim</sub>	UPR
OmniPhysGS	0.2149	86%	0.2291	78%	0.2135	74%	0.1834	80%	0.2047	62%	0.2091	76%
DreamPhysics	0.2273	88%	0.2459	64%	0.2437	68%	0.2071	72%	0.2217	78%	0.2291	74%
PhysGM (w/o DPO)	0.2698	58%	0.2700	54%	0.2547	60%	0.2541	52%	0.2980	62%	0.2693	57%
PhysGM (w/ DPO)	<b>0.2732</b>	-	<b>0.2774</b>	-	<b>0.2691</b>	-	<b>0.2548</b>	-	<b>0.2997</b>	-	<b>0.2748</b>	-

Table 1: Quantitative comparisons. We evaluate our method and baseline models on 5 different material types. Evaluation is based on the CLIP<sub>sim</sub> score (higher is better  $\uparrow$ ) and UPR (lower is better  $\downarrow$ ).

Method (MPM) simulation. The predicted material class determines which **constitutive model** is employed to govern the object’s dynamic behavior. For instance, a prediction of ‘rubber’ would select a Neo-Hookean constitutive model. The predicted Young’s modulus ( $E$ ) and Poisson’s ratio ( $\nu$ ) then serve as the specific parameters for this chosen model. We use a fixed sub-step time of  $2 \times 10^{-5}$ s and a frame time of  $4 \times 10^{-2}$ s, generating 50 frames per sequence. Additional simulation parameters, such as boundary conditions, are detailed in the Appendix.

**Training Details** We initialize our model with the weight of LGM (Tang et al. 2024). We train our model for 12 hours on 8 NVIDIA A800 GPUs, with a batch size of 8 per GPU. The training process is conducted in two stages. In the pre-training phase, we jointly optimize our model for physics and Gaussian prediction under the supervision of PhysAssets. In the fine-tuning stage, we apply DPO to guide the model to generate more physically realistic dynamics. During this stage, we freeze the backbone of the model, fine-tuning only the predictive heads for Gaussian parameters and physics properties.

**Evaluation Metrics** We conduct a comprehensive evaluation using two complementary metrics: an objective, model-based score and a subjective, human-based assessment. (1) CLIP<sub>sim</sub> (Radford et al. 2021) quantifies the semantic similarity between the rendered visual outcomes and their corresponding textual descriptions of the physical phenomena. (2) User Preference Rate (UPR). We conduct a Two-Alternative Forced-Choice (2AFC) user study. The participants are presented with side-by-side results from our method and a competitor, asked to select the more realistic or visually appealing one. UPR is defined as the percentage of trials where our method was chosen.

## Results and Analysis

In this section, we empirically validate the effectiveness of PhysGM. We conduct a comprehensive comparison against baseline methods, and a targeted ablation study to isolate the contributions of our two-stage training paradigm.

**Comparison with baseline methods** We begin by showcasing the core capability of optimization-free 4D generation. As illustrated in Figure 4, our model takes a single input image and, in a single feed-forward pass, generates a complete 3D Gaussian representation along with its corre-

sponding physical properties. This allows for the production of a full, physically based simulation in under one minute.

For a quantitative comparison, we evaluate PhysGM against two optimization-based baselines, OmniPhysGS and DreamerPhysics. Our method outperforms both baselines on both metrics across a diverse range of materials. This result demonstrates that our feed-forward approach does not merely trade quality for speed. Instead, by learning a robust physical prior from a large dataset, PhysGM can surpass the perceptual realism and physical plausibility of slower, per-scene optimization techniques.

**Ablation Study** To validate the effectiveness of our proposed two-stage training strategy, we conduct an ablation study focused on the DPO fine-tuning stage. We compare our full PhysGM model against a baseline variant, “w/o DPO,” which is trained exclusively with supervised pre-training and does not undergo DPO refinement.

The results presented in Table 1 and visualized in Figure 5 clearly demonstrate the critical role of the DPO stage. The full model achieves substantially higher scores across all categories in both metrics. The qualitative comparison is particularly revealing. While the pretraining-only model might predict a plausible but overly rigid material, the DPO-refined model learns to predict more accurate physical parameters. This leads to simulations with significantly more natural deformations. These findings confirm that our DPO refinement stage is essential for transforming a statistically sound prior into a perceptually better generative model. It effectively uses the feedback from the entire simulation pipeline, steering the model towards outputs that are not just statistically likely but are physically and visually more compelling.

## Conclusion

We presented **PhysGM**, a feed-forward framework for rapid, physically grounded 4D synthesis from sparse inputs. Our model is first optimized for 3D Gaussian reconstruction and physical properties prediction, then finetuned with Direct Preference Optimization (DPO) to learn from a non-differentiable simulator, eliminating the need for per-scene optimization. Empirical analysis reveals our approach yields physically realistic simulation and rendering in under a minute. PhysGM’s efficiency paves the way for scalable applications in embodied AI, autonomous driving, and interactive virtual reality.

## References

- Bahmani, S.; Skorokhodov, I.; Rong, V.; Wetzstein, G.; Guibas, L.; Wonka, P.; Tulyakov, S.; Park, J. J.; Tagliasacchi, A.; and Lindell, D. B. 2024. 4d-fy: Text-to-4d generation using hybrid score distillation sampling. In *Proceedings of the IEEE/CVF Conference on Computer Vision and Pattern Recognition*, 7996–8006.
- Cai, J.; Yang, Y.; Yuan, W.; He, Y.; Dong, Z.; Bo, L.; Cheng, H.; and Chen, Q. 2024. Gic: Gaussian-informed continuum for physical property identification and simulation. *Advances in Neural Information Processing Systems*, 37: 75035–75063.
- Cao, Z.; Chen, Z.; Pan, L.; and Liu, Z. 2025. PhysX: Physical-Grounded 3D Asset Generation. *arXiv preprint arXiv:2507.12465*.
- Charatan, D.; Li, S. L.; Tagliasacchi, A.; and Sitzmann, V. 2024. pixelsplat: 3d gaussian splats from image pairs for scalable generalizable 3d reconstruction. In *Proceedings of the IEEE/CVF conference on computer vision and pattern recognition*, 19457–19467.
- Chen, B.; Jiang, H.; Liu, S.; Gupta, S.; Li, Y.; Zhao, H.; and Wang, S. 2025. Physgen3d: Crafting a miniature interactive world from a single image. In *Proceedings of the Computer Vision and Pattern Recognition Conference*, 6178–6189.
- Chen, Y.; Xu, H.; Zheng, C.; Zhuang, B.; Pollefeys, M.; Geiger, A.; Cham, T.-J.; and Cai, J. 2024. Mvsplat: Efficient 3d gaussian splatting from sparse multi-view images. In *European Conference on Computer Vision*, 370–386. Springer.
- Collins, J.; Goel, S.; Deng, K.; Luthra, A.; Xu, L.; Gundogdu, E.; Zhang, X.; Vicente, T. F. Y.; Dideriksen, T.; Arora, H.; et al. 2022. Abo: Dataset and benchmarks for real-world 3d object understanding. In *Proceedings of the IEEE/CVF conference on computer vision and pattern recognition*, 21126–21136.
- Deitke, M.; Schwenk, D.; Salvador, J.; Weihs, L.; Michel, O.; VanderBilt, E.; Schmidt, L.; Ehsani, K.; Kembhavi, A.; and Farhadi, A. 2023. Objaverse: A universe of annotated 3d objects. In *Proceedings of the IEEE/CVF conference on computer vision and pattern recognition*, 13142–13153.
- Downs, L.; Francis, A.; Koenig, N.; Kinman, B.; Hickman, R.; Reymann, K.; McHugh, T. B.; and Vanhoucke, V. 2022. Google scanned objects: A high-quality dataset of 3d scanned household items. In *2022 International Conference on Robotics and Automation (ICRA)*, 2553–2560. IEEE.
- Hong, Y.; Zhang, K.; Gu, J.; Bi, S.; Zhou, Y.; Liu, D.; Liu, F.; Sunkavalli, K.; Bui, T.; and Tan, H. 2023. Lrm: Large reconstruction model for single image to 3d. *arXiv preprint arXiv:2311.04400*.
- Huang, T.; Zhang, H.; Zeng, Y.; Zhang, Z.; Li, H.; Zuo, W.; and Lau, R. W. 2025. DreamPhysics: Learning Physics-Based 3D Dynamics with Video Diffusion Priors. In *Proceedings of the AAAI Conference on Artificial Intelligence*, volume 39, 3733–3741.
- Jiang, C.; Schroeder, C.; Teran, J.; Stomakhin, A.; and Selle, A. 2016. The material point method for simulating continuum materials. In *Acm siggraph 2016 courses*, 1–52.
- Jiang, Y.; Yu, C.; Cao, C.; Wang, F.; Hu, W.; and Gao, J. 2024. Animate3d: Animating any 3d model with multi-view video diffusion. *Advances in Neural Information Processing Systems*, 37: 125879–125906.
- Jun, H.; and Nichol, A. 2023. Shap-e: Generating conditional 3d implicit functions. *arXiv preprint arXiv:2305.02463*.
- Karaev, N.; Makarov, I.; Wang, J.; Neverova, N.; Vedaldi, A.; and Rupprecht, C. 2024a. CoTracker3: Simpler and Better Point Tracking by Pseudo-Labeling Real Videos. In *Proc. arXiv:2410.11831*.
- Karaev, N.; Rocco, I.; Graham, B.; Neverova, N.; Vedaldi, A.; and Rupprecht, C. 2024b. Cotracker: It is better to track together. In *European conference on computer vision*, 18–35. Springer.
- Kerbl, B.; Kopanas, G.; Leimkühler, T.; and Drettakis, G. 2023. 3D Gaussian splatting for real-time radiance field rendering. *ACM Trans. Graph.*, 42(4): 139–1.
- Kirillov, A.; Mintun, E.; Ravi, N.; Mao, H.; Rolland, C.; Gustafson, L.; Xiao, T.; Whitehead, S.; Berg, A. C.; Lo, W.-Y.; et al. 2023. Segment anything. In *Proceedings of the IEEE/CVF international conference on computer vision*, 4015–4026.
- Li, J.; Tan, H.; Zhang, K.; Xu, Z.; Luan, F.; Xu, Y.; Hong, Y.; Sunkavalli, K.; Shakhnarovich, G.; and Bi, S. 2023. Instant3d: Fast text-to-3d with sparse-view generation and large reconstruction model. *arXiv preprint arXiv:2311.06214*.
- Lin, Y.; Lin, C.; Xu, J.; and Mu, Y. 2025. OmniphysGS: 3d constitutive gaussians for general physics-based dynamics generation. *arXiv preprint arXiv:2501.18982*.
- Ling, H.; Kim, S. W.; Torralba, A.; Fidler, S.; and Kreis, K. 2024. Align your gaussians: Text-to-4d with dynamic 3d gaussians and composed diffusion models. In *Proceedings of the IEEE/CVF conference on computer vision and pattern recognition*, 8576–8588.
- Liu, F.; Wang, H.; Yao, S.; Zhang, S.; Zhou, J.; and Duan, Y. 2024a. Physics3d: Learning physical properties of 3d gaussians via video diffusion. *arXiv preprint arXiv:2406.04338*.
- Liu, S.; Ren, Z.; Gupta, S.; and Wang, S. 2024b. Physgen: Rigid-body physics-grounded image-to-video generation. In *European Conference on Computer Vision*, 360–378. Springer.
- Lu, G.; Zhang, S.; Wang, Z.; Liu, C.; Lu, J.; and Tang, Y. 2024. ManiGaussian: Dynamic Gaussian Splatting for Multi-task Robotic Manipulation. *arXiv preprint arXiv:2403.08321*.
- Macklin, M. 2022. Warp: A high-performance python framework for gpu simulation and graphics. In *NVIDIA GPU Technology Conference (GTC)*, volume 3.
- Nichol, A.; Jun, H.; Dhariwal, P.; Mishkin, P.; and Chen, M. 2022. Point-e: A system for generating 3d point clouds from complex prompts. *arXiv preprint arXiv:2212.08751*.
- Pan, Z.; Yang, Z.; Zhu, X.; and Zhang, L. 2024. Efficient4d: Fast dynamic 3d object generation from a single-view video. *arXiv preprint arXiv:2401.08742*.



- Park, J. J.; Florence, P.; Straub, J.; Newcombe, R.; and Lovegrove, S. 2019. DeepSDF: Learning continuous signed distance functions for shape representation. In *Proceedings of the IEEE/CVF conference on computer vision and pattern recognition*, 165–174.
- Poole, B.; Jain, A.; Barron, J. T.; and Mildenhall, B. 2022. DreamFusion: Text-to-3d using 2d diffusion. *arXiv preprint arXiv:2209.14988*.
- Qiu, R.-Z.; Yang, G.; Zeng, W.; and Wang, X. 2024. Feature splatting: Language-driven physics-based scene synthesis and editing. *arXiv preprint arXiv:2404.01223*.
- Radford, A.; Kim, J. W.; Hallacy, C.; Ramesh, A.; Goh, G.; Agarwal, S.; Sastry, G.; Askell, A.; Mishkin, P.; Clark, J.; et al. 2021. Learning transferable visual models from natural language supervision. In *International conference on machine learning*, 8748–8763. PMLR.
- Rafailov, R.; Sharma, A.; Mitchell, E.; Manning, C. D.; Ermon, S.; and Finn, C. 2023. Direct preference optimization: Your language model is secretly a reward model. *Advances in neural information processing systems*, 36: 53728–53741.
- Ravi, N.; Gabeur, V.; Hu, Y.-T.; Hu, R.; Ryali, C.; Ma, T.; Khedr, H.; Rädle, R.; Rolland, C.; Gustafson, L.; et al. 2024. Sam 2: Segment anything in images and videos. *arXiv preprint arXiv:2408.00714*.
- Ren, J.; Pan, L.; Tang, J.; Zhang, C.; Cao, A.; Zeng, G.; and Liu, Z. 2023. Dreamgaussian4d: Generative 4d gaussian splatting. *arXiv preprint arXiv:2312.17142*.
- Ren, J.; Xie, C.; Mirzaei, A.; Kreis, K.; Liu, Z.; Torralba, A.; Fidler, S.; Kim, S. W.; Ling, H.; et al. 2024. L4gm: Large 4d gaussian reconstruction model. *Advances in Neural Information Processing Systems*, 37: 56828–56858.
- Shi, Y.; Wang, P.; Ye, J.; Mai, L.; Li, K.; and Yang, X. 2023. MVDream: Multi-view Diffusion for 3D Generation. *arXiv:2308.16512*.
- Stomakhin, A.; Schroeder, C.; Chai, L.; Teran, J.; and Selle, A. 2013. A material point method for snow simulation. *ACM Transactions on Graphics (TOG)*, 32(4): 1–10.
- Szymanowicz, S.; Rupprecht, C.; and Vedaldi, A. 2024. Splatler image: Ultra-fast single-view 3d reconstruction. In *Proceedings of the IEEE/CVF conference on computer vision and pattern recognition*, 10208–10217.
- Tan, X.; Jiang, Y.; Li, X.; Zong, Z.; Xie, T.; Yang, Y.; and Jiang, C. 2024. Physmotion: Physics-grounded dynamics from a single image. *arXiv preprint arXiv:2411.17189*.
- Tang, J.; Chen, Z.; Chen, X.; Wang, T.; Zeng, G.; and Liu, Z. 2024. Lgm: Large multi-view gaussian model for high-resolution 3d content creation. In *European Conference on Computer Vision*, 1–18. Springer.
- Tschannen, M.; Gritsenko, A.; Wang, X.; Naeem, M. F.; Alabdulmohsin, I.; Parthasarathy, N.; Evans, T.; Beyer, L.; Xia, Y.; Mustafa, B.; et al. 2025. Siglip 2: Multilingual vision-language encoders with improved semantic understanding, localization, and dense features. *arXiv preprint arXiv:2502.14786*.
- Wang, J.; Yuan, H.; Chen, D.; Zhang, Y.; Wang, X.; and Zhang, S. 2023a. Modelscope text-to-video technical report. *arXiv preprint arXiv:2308.06571*.
- Wang, P.; Tan, H.; Bi, S.; Xu, Y.; Luan, F.; Sunkavalli, K.; Wang, W.; Xu, Z.; and Zhang, K. 2023b. Pf-lrm: Pose-free large reconstruction model for joint pose and shape prediction. *arXiv preprint arXiv:2311.12024*.
- Wu, S.; Lin, Y.; Zhang, F.; Zeng, Y.; Xu, J.; Torr, P.; Cao, X.; and Yao, Y. 2024. Direct3d: Scalable image-to-3d generation via 3d latent diffusion transformer. *Advances in Neural Information Processing Systems*, 37: 121859–121881.
- Wu, T.; Zhang, J.; Fu, X.; Wang, Y.; Ren, J.; Pan, L.; Wu, W.; Yang, L.; Wang, J.; Qian, C.; et al. 2023. Omniobject3d: Large-vocabulary 3d object dataset for realistic perception, reconstruction and generation. In *Proceedings of the IEEE/CVF Conference on Computer Vision and Pattern Recognition*, 803–814.
- Xie, T.; Zong, Z.; Qiu, Y.; Li, X.; Feng, Y.; Yang, Y.; and Jiang, C. 2024. Physgaussian: Physics-integrated 3d gaussians for generative dynamics. In *Proceedings of the IEEE/CVF Conference on Computer Vision and Pattern Recognition*, 4389–4398.
- Xu, Y.; Shi, Z.; Yifan, W.; Chen, H.; Yang, C.; Peng, S.; Shen, Y.; and Wetzstein, G. 2024. Grm: Large gaussian reconstruction model for efficient 3d reconstruction and generation. In *European Conference on Computer Vision*, 1–20. Springer.
- Yin, Y.; Xu, D.; Wang, Z.; Zhao, Y.; and Wei, Y. 2023. 4dgen: Grounded 4d content generation with spatial-temporal consistency. *arXiv preprint arXiv:2312.17225*.
- Zhang, H.; Chen, X.; Wang, Y.; Liu, X.; Wang, Y.; and Qiao, Y. 2024a. 4diffusion: Multi-view video diffusion model for 4d generation. *Advances in Neural Information Processing Systems*, 37: 15272–15295.
- Zhang, K.; Bi, S.; Tan, H.; Xiangli, Y.; Zhao, N.; Sunkavalli, K.; and Xu, Z. 2024b. Gs-lrm: Large reconstruction model for 3d gaussian splatting. In *European Conference on Computer Vision*, 1–19. Springer.
- Zhang, L.; and Agrawala, M. 2025. Packing input frame context in next-frame prediction models for video generation. *arXiv preprint arXiv:2504.12626*.
- Zhang, T.; Yu, H.-X.; Wu, R.; Feng, B. Y.; Zheng, C.; Snavely, N.; Wu, J.; and Freeman, W. T. 2024c. Physdreamer: Physics-based interaction with 3d objects via video generation. In *European Conference on Computer Vision*, 388–406. Springer.
- Zhao, H.; Wang, H.; Zhao, X.; Fei, H.; Wang, H.; Long, C.; and Zou, H. 2024. Efficient Physics Simulation for 3D Scenes via MLLM-Guided Gaussian Splatting. *arXiv preprint arXiv:2411.12789*.
- Zhou, X.; Lin, Z.; Shan, X.; Wang, Y.; Sun, D.; and Yang, M.-H. 2024. Drivinggaussian: Composite gaussian splatting for surrounding dynamic autonomous driving scenes. In *Proceedings of the IEEE/CVF conference on computer vision and pattern recognition*, 21634–21643.

# Supplementary Materials

## More Details on Implementation

### Compare with Other Methods

Table 2 provides a qualitative comparison between our method, PhysGM, and other state-of-the-art approaches (Xie et al. 2024; Zhang et al. 2024c; Huang et al. 2025; Lin et al. 2025; Ren et al. 2023; Qiu et al. 2024; Zhao et al. 2024). We evaluate each method across five critical dimensions: two concerning input requirements (the need for pre-optimized 3D Gaussians or pre-defined physical parameter) and three concerning core capabilities (generalizability, independence from Large Language Models, and inference speed). The comparison highlights that our approach is the only one to operate without these stringent prerequisites. PhysGM simultaneously achieves strong generalization and maintains a very short inference time of under 30 seconds.

### Simulation Details

This section elaborates on the key parameters used to configure our Material Point Method (MPM) simulations, as referenced in the main text. The configuration is detailed below, categorized by function.

**MPM Grid Resolution:** The simulation domain is discretized into a background grid of  $200 * 200 * 200$  cells. This grid is fundamental to the MPM algorithm for computing particle interactions and mapping data between particles and the grid.

**Camera Motion:** The camera is configured to be static during the simulation.

**Other Parameters:** Gravity is applied in the falling scene, and force in the corresponding direction is applied in the collision scene.

### Training Details

We train our model on 8 NVIDIA A800 GPUs using a two-stage process for 12 hours in total. The stage one consisted of 30 epochs, and the stage two consisted of 20 epochs. We employed the AdamW optimizer with a learning rate of  $1e-6$  and applied gradient clipping with a maximum norm of 1.0. For data augmentation, both grid distortion and camera jitter were applied with a probability of 50%.

## Material Constitutive Models

In continuum mechanics and physics-based simulation, a constitutive model (or constitutive equation) is a fundamental mathematical relationship that describes how a material responds to external stimuli. Specifically, it defines the relationship between the internal forces (stress) and the material’s deformation (strain). The choice of a constitutive model is critical as it dictates the material’s behavior—whether it behaves as a rigid solid, an elastic solid, a fluid, or a hyperelastic material like rubber. Our simulation framework employs different constitutive models based on the predicted material class. This allows us to capture a diverse range of dynamic behaviors.

## The Neo-Hookean Model

For materials predicted to be “jelly” or other soft, rubber-like substances, we employ the Neo-Hookean model. This is a classic hyperelastic model, meaning its stress-response is derived from a strain energy density function. It is ideal for capturing large, nonlinear deformations while remaining computationally efficient, making it a staple in computer graphics and simulation. The model’s formulation is based on the statistical mechanics of polymer chains, which accurately describes the behavior of materials like rubber that can stretch significantly without permanent deformation.

The core idea is to split the material’s response into two parts: a part that resists changes in shape (deviatoric) and a part that resists changes in volume (volumetric). This allows for a robust simulation of compressible, soft-bodied dynamics. The model defines the Kirchhoff stress ( $\tau$ ), which is a measure of internal force suitable for large-deformation analysis. The Kirchhoff stress  $\tau$  for a compressible Neo-Hookean material is given by:

$$\tau = \mu * J^{-2/3} * \text{dev}(\mathbf{B}) + (\lambda/2) * (J^2 - 1) * \mathbf{I}, \quad (12)$$

where  $\tau$  is the Kirchhoff stress tensor.  $\mathbf{B} = \mathbf{F}\mathbf{F}^T$  is the left Cauchy-Green deformation tensor, where  $\mathbf{F}$  is the deformation gradient and  $\text{dev}(\mathbf{B})$  is the deviatoric (volume-preserving) part of  $\mathbf{B}$ .  $J = \det(\mathbf{F})$  is the determinant of the deformation gradient, representing the volume change.  $\mu$  and  $\lambda$  are the Lamé parameters, which characterize the material’s stiffness. They are derived from the Young’s modulus ( $E$ ) and Poisson’s ratio ( $\nu$ ) predicted by our model.

## The Fixed Corotational Constitutive Model

For materials predicted to be “metal” or other similarly stiff elastic solids, we employ the Fixed Corotational (FCR) constitutive model. This model is particularly well-suited for scenarios where a material undergoes large rigid-body motions (i.e., translation and rotation) but experiences only small elastic deformations. The core principle of any corotational model is to decouple the object’s overall rotation from its internal strain. The FCR model begins with the polar decomposition of the deformation gradient  $\mathbf{F} = \mathbf{R}\mathbf{S}$ , where  $\mathbf{R}$  is a pure rotation matrix, and  $\mathbf{S}$  is the right stretch tensor, which is symmetric and positive definite. The model defines a linear relationship between the First Piola-Kirchhoff stress ( $\mathbf{P}$ ) and a measure of strain. The First Piola-Kirchhoff stress is energetically conjugate to the deformation gradient  $\mathbf{F}$  and is given by:

$$\mathbf{P} = 2\mu(\mathbf{F} - \mathbf{R}) + \lambda(J - 1)J(\mathbf{F}^{-T}), \quad (13)$$

where  $\mathbf{P}$  is the First Piola-Kirchhoff stress tensor. For force calculations within our MPM simulation, we use the Kirchhoff stress ( $\tau$ ). The relationship between Kirchhoff stress and the First Piola-Kirchhoff stress is:  $\tau = \mathbf{P}\mathbf{F}^T$ .

## The Drucker-Prager Plasticity Model

For materials exhibiting both frictional and cohesive properties, such as sand, snow, and plasticine, we employ the Drucker-Prager elastoplasticity model. This model is ideal for materials whose strength is dependent on the hydrostatic

Table 2: Comparison with state-of-the-art methods, highlighting PhysGM’s unique advantages. Unlike prior work, our method eliminates the need for both pre-optimized 3D Gaussian and pre-defined physical parameters. This allows it to achieve strong generalization while maintaining a significantly shorter inference time ( $< 30s$ ). “only E” represents that only Young’s modulus is automatically predicted, “only material” represents that only material is automatically predicted.

Method	No Pre-opt. 3D Gaussians	Auto Param Computation	Generalizable	Without LLM	Inference Time
PhysGaussian (Xie et al. 2024)	×	×	×	✓	-
DreamPhysics (Huang et al. 2025)	×	only E	×	✓	$>0.5h$
PhysDreamer (Zhang et al. 2024c)	×	only E	×	✓	$>1h$
OmniPhysGS (Lin et al. 2025)	×	only material	×	✓	$>12h$
DreamGaussian4D (Ren et al. 2023)	✓	×	✓	×	6.5min
Feature Splatting (Qiu et al. 2024)	×	×	×	✓	$>1h$
PhysSplat (Zhao et al. 2024)	×	✓	✓	×	$<2min$
<b>PhysGM (Ours)</b>	✓	✓	✓	✓	<b><math>&lt;30s</math></b>

pressure they are under (e.g., sand becomes stronger when compressed). It defines a yield criterion, which is a surface in stress space that separates elastic (temporary) deformation from plastic (permanent) deformation. The core of the model is the predictor-corrector algorithm, also known as return mapping: First, the model assumes the material behaves purely elastically during a time step and calculates a “trial stress”. It then checks if this trial stress lies outside the Drucker-Prager yield surface. If the trial stress is outside the surface (i.e., the material has yielded), the stress is mathematically projected back onto the yield surface. This correction step accounts for the plastic flow and ensures the material’s stress state remains physically plausible. The Drucker-Prager yield criterion defines the boundary between elastic and plastic states. The yield function is given by:

$$f(\tau) = ||\text{dev}(\tau)|| + \alpha * \text{tr}(\tau) - k \leq 0, \quad (14)$$

where  $\tau$  is the Kirchhoff stress tensor.  $\text{dev}(\tau)$  is the deviatoric part of the stress, representing shear.  $||\text{dev}(\tau)||$  is the Frobenius norm of the deviatoric stress, measuring the magnitude of the shear stress.  $\text{tr}(\tau)$  is the trace of the stress, proportional to the hydrostatic pressure (positive for tension, negative for compression).  $\alpha$  is a dimensionless friction parameter, controlling how much the material’s strength increases with pressure.  $k$  is the cohesion of the material, representing its intrinsic shear strength at zero pressure.

The key insight is that different materials like sand, snow, and plasticine can be simulated with the same underlying model by simply adjusting the cohesion ( $k$ ) and friction ( $\alpha$ ) parameters. For instance: Sand ( $k = 0.0$ ) has negligible cohesion; its strength comes almost entirely from inter-particle friction. Snow ( $k = 1000.0$ ) represents an intermediate case with some cohesion. Plasticine ( $k = 5000.0$ ) has significant cohesion, allowing it to hold its shape even without compressive pressure.

## Dataset

This section provides a detailed account of the construction process for our PhysAssets Dataset, which serves as the foundation for our research. The final dataset comprises over 24,000 unique 3D objects, meticulously curated and integrated from four prominent existing datasets: OmniObject3D (Wu et al. 2023), Google Scanned Objects (GSO) (Downs et al. 2022), Amazon Berkeley Objects (ABO) (Collins et al. 2022), and Objaverse (Deitke et al. 2023). The primary objective of this effort was to create a comprehensive, diverse, and standardized collection of Physical-based assets annotated with four-view rendered images, physical properties, and corresponding guiding videos.

### Source Datasets

Our dataset aggregates models from the following four sources, each contributing unique characteristics:

**OmniObject3D** A high-fidelity dataset featuring approximately 6,000 real-world scanned objects across 190 common categories (e.g., cups, chairs, animal models). It provides rich multi-modal data, including textured meshes with millimeter-level geometric accuracy and multi-view rendered images. For our purposes, we primarily leveraged its high-resolution rendered views (e.g., the 24-view set with associated camera parameters) to extract detailed appearance and geometric information.

**Google Scanned Objects (GSO)** This dataset contains 1,030 photorealistic 3D models of common household items, such as kitchenware, stationery, and electronics. The models are provided as textured meshes (.obj, .mtl) and include pre-rendered orthogonal views (front, back, left, right), which facilitate standardized data extraction for our pipeline.

**Amazon Berkeley Objects (ABO)** ABO offers a collection of approximately 8,000 high-quality, industry-standard 3D models covering 98 everyday object categories. The data

includes textured CAD models (.obj/.glb), which we utilized to generate consistent multi-view renderings that align with our standardized format.

**Objaverse** A 10M+ dataset containing millions of 3D objects, Objaverse offers unparalleled diversity in object shape, category, and style. We selected a substantial subset from this collection to significantly broaden the scope and variety of our final dataset, as detailed in the following section.

## Data Processing

**Filter and Render** To ensure quality and consistency across the heterogeneous source datasets, we established a systematic data curation and processing pipeline. The Objaverse dataset, while extensive, is characterized by its considerable size and variable data quality. Consequently, to extract a high-quality subset, we employed a systematic curation strategy analogous to the one applied to gobjaverse. The screening procedure is outlined as follows: (1) A geometric similarity clustering algorithm was employed to identify and remove near-duplicate models. Any model exhibiting a similarity score of over 85% with another was considered redundant and removed; (2) To filter out objects with non-standard or incomplete textures, we performed an analysis in the HSV (Hue, Saturation, Value) color space. Models where white pixels constituted more than 75% of the surface texture were discarded, as this often indicates missing or placeholder textures. In the end, we filtered approximately 10k data points in the Objaverse. For the other datasets, we used the full data without applying a filtering process. For datasets that do not provide a four view rendering view, we use the rendering script provided by the corresponding dataset for four view rendering. This procedure ensures that every object in our dataset is represented by a consistent set of views, capturing its complete geometric features for subsequent learning tasks.

**Physical Property Annotation** We employ a vision-language joint modeling approach for material classification. The four orthogonal RGB images of each object are fed into a pre-trained SigLIP-2 model. This model calculates the cross-modal similarity between the object’s visual features and the textual descriptions of seventeen common materials (e.g., “wood”, “metal”, “plasticine”). The final material label for each object is determined via a weighted voting mechanism based on these similarity scores. The prediction of mechanical parameters, specifically Young’s modulus and the Poisson’s ratio, is achieved through a similar methodology. Once a material is identified, its density value (in  $\text{g/cm}^3$ ) is assigned using a layered mapping framework that correlates the material label with standard physical constants.

## Video Generation and Preference Calculation Process

To facilitate the second stage of our training, which employs Direct Preference Optimization (DPO), we established a systematic pipeline for generating a large-scale dataset of preference tuples. This process is crucial for providing the high-quality, ranked data required to fine-tune our model on

the nuances of physical dynamics. The pipeline consists of three main steps:

**Ground-Truth Videos Generation** For some scenes in our dataset, we generate a high-fidelity, ground-truth simulation video. This is achieved by utilizing FramePack, a video generation model, which is guided by a unique, descriptive prompt for each material and then manually selected. These prompts define the initial conditions and interactions, ensuring the resulting video serves as an authoritative benchmark for both physical accuracy and visual realism.

**Candidate Video Generation** Leveraging the model pre-trained in Stage 1, we generate a set of plausible, yet varied, simulation outcomes. Specifically, we sample three distinct sets of physical properties (e.g., Young’s modulus, Poisson’s ratio) from the learned probability distribution associated with the object. Each of these property sets is then used to run a new simulation, producing three unique candidate videos that represent different potential physical behaviors.

**Automated Ranking and Preference Pair Construction** To automate the preference labeling process, we implement a quantitative comparison method. We employ CoTracker-3, a state-of-the-art model for dense point tracking, to trace the trajectories of a predefined set of pixels across the ground-truth video and each of the three candidate videos. The physical and perceptual similarity between each candidate and the ground truth is quantified by calculating the L2 distance (Euclidean distance) between their corresponding pixel trajectories. A lower L2 distance signifies a closer match to the ground-truth motion, indicating higher physical fidelity. Based on the calculated L2 distances, we establish a definitive preference ranking (e.g., Candidate A > Candidate B > Candidate C, where A has the lowest L2 distance). This ranked list is subsequently decomposed into multiple (winner, loser) preference pairs. The resulting collection of pairs forms the final dataset that directly fuels our DPO fine-tuning, enabling the model to discern and internalize the subtle principles governing realistic physical dynamics.

**Additional Data Sources** It is also worth noting that the PhysX (Cao et al. 2025) dataset was released concurrently with our research, offering 3D objects annotated with physical properties, which is also suitable for our dataset process. Given the timing constraints, its integration was not feasible for the present study. Nevertheless, we acknowledge its significance and view it as a promising avenue for extending our work in the future.

## Additional Results

To demonstrate the versatility and robustness of our approach, we present a range of additional experiments. We showcase qualitative results for fundamental stretching and dropping scenarios in Figure 6 and Figure 7, respectively. These experiments are further extended to demonstrate our model’s performance across more challenging configurations: Figure 8 illustrates its robustness in scenes with complex backgrounds, while Figure 9 highlights its capability to handle multi-object interactions. Additional results are presented in the Figure 10 Figure 11 Figure 12.



## Limitations and Future Work

While PhysGM demonstrates significant advances in fast, physically-grounded 3D synthesis, it is important to acknowledge its current limitations, which also highlight promising directions for future research.

**Data Dependency and Generalization.** Our model’s performance is inherently tied to the scope and diversity of the PhysAssets dataset. While large, the dataset primarily consists of rigid objects. Consequently, the model may not generalize well to out-of-distribution categories, such as highly deformable or articulated objects. Future work could focus on expanding the dataset and exploring domain adaptation techniques to handle a wider variety of object types.

**Simplified Physics Representation.** PhysGM currently predicts a single, “lumped” vector of physical properties (e.g., one mass, one friction coefficient) for the entire object. This assumes uniform material composition, which is not true for many real-world objects (e.g., a hammer with a metal head and wooden handle). A significant next step would be to extend our framework to predict spatially varying material properties, enabling more complex and realistic simulations.

**Limitations of Base Models.** Our method for 3D reconstruction primarily relies on LGM and MVDream as its foundational models. While these models perform effectively in most scenarios, their inherent limitations can still impact the quality of the final output, potentially leading to issues such as the loss of geometric detail, the introduction of artifacts, or textural inconsistencies. Consequently, a key direction for future work is to explore and integrate more advanced and robust generative models as replacements.



Figure 6: Qualitative results for stretching scenarios. Our method correctly captures the distinct responses of different materials under tensile forces.

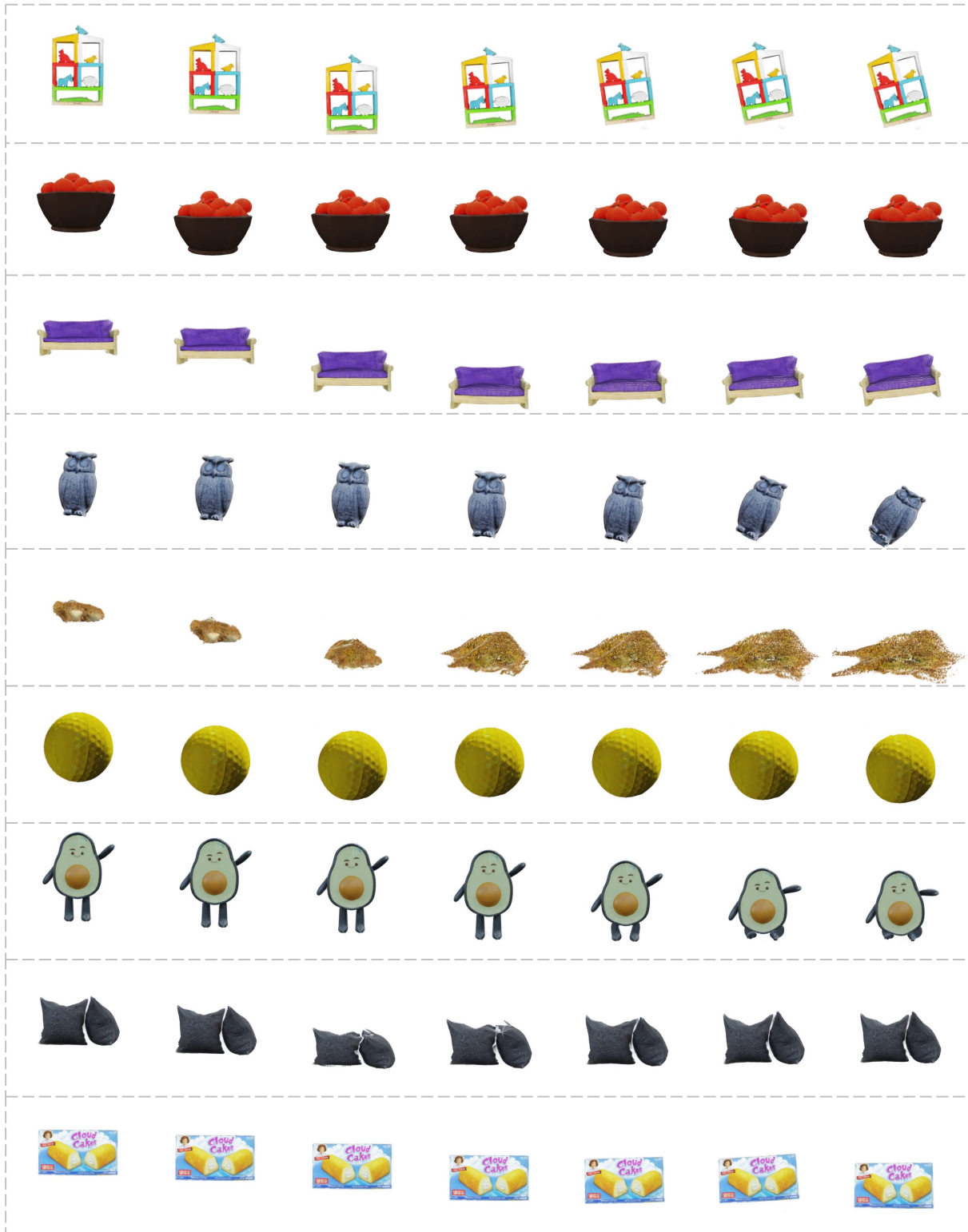


Figure 7: Qualitative results for dropping scenarios. Our model accurately predicts the physical properties of different materials, leading to plausible deformation and final states upon impact with the ground.



Figure 8: Demonstration of our model’s robustness in in-the-wild scenes.



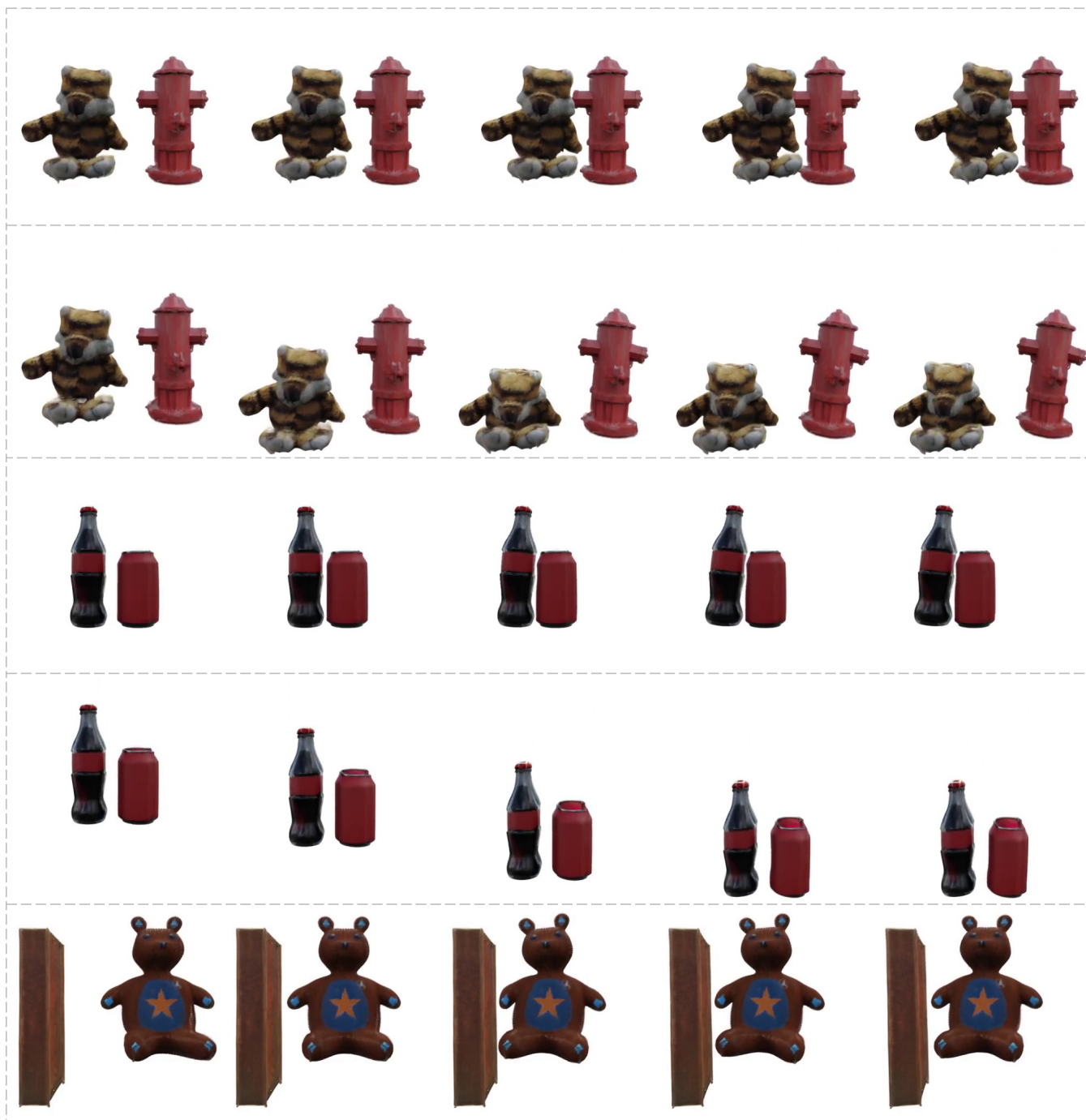


Figure 9: Qualitative results for multi-object interaction scenarios. Our approach can handle more complex scenes involving simultaneous collisions and interactions, generating physically consistent outcomes for all objects.

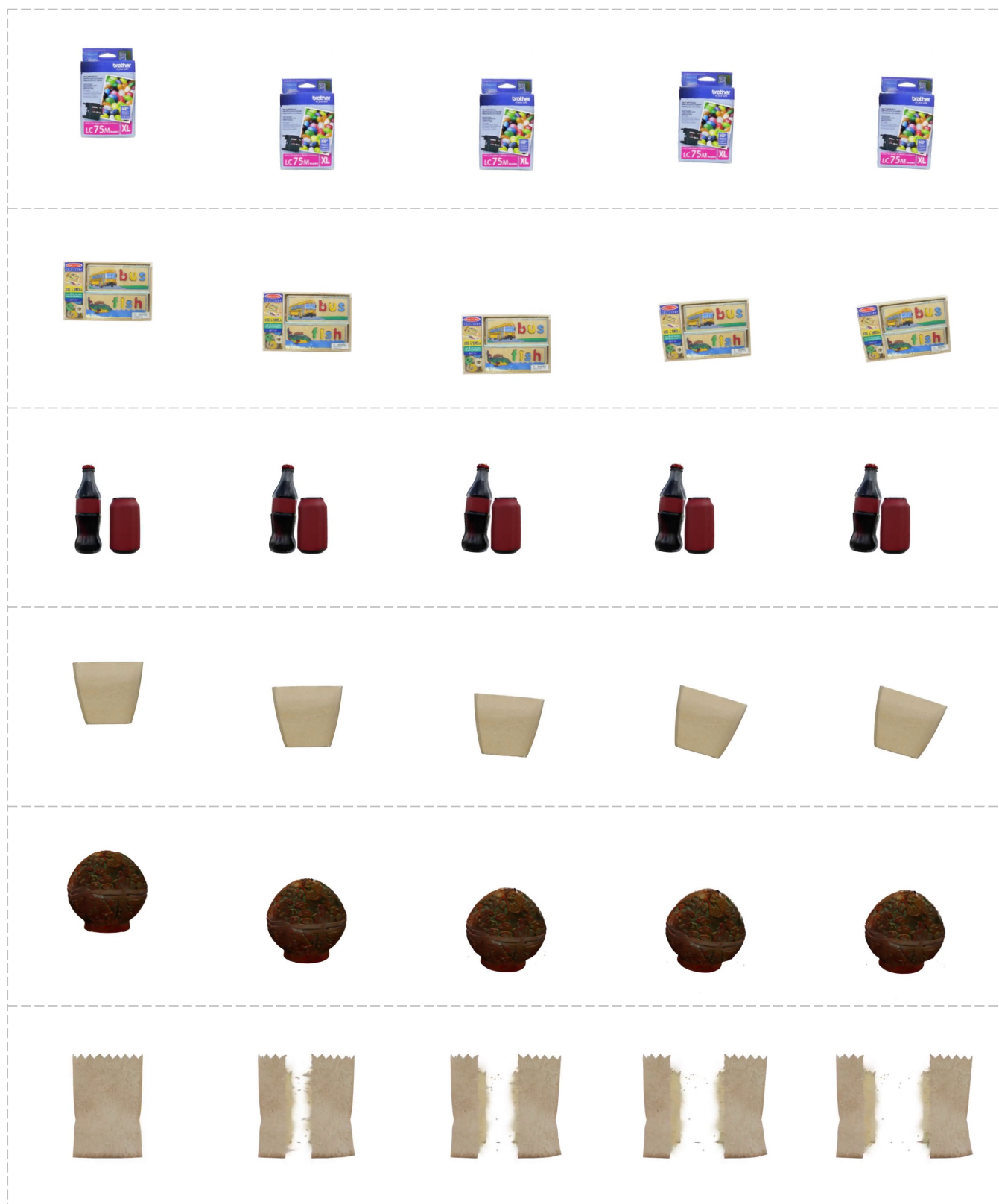


Figure 10: Other results.

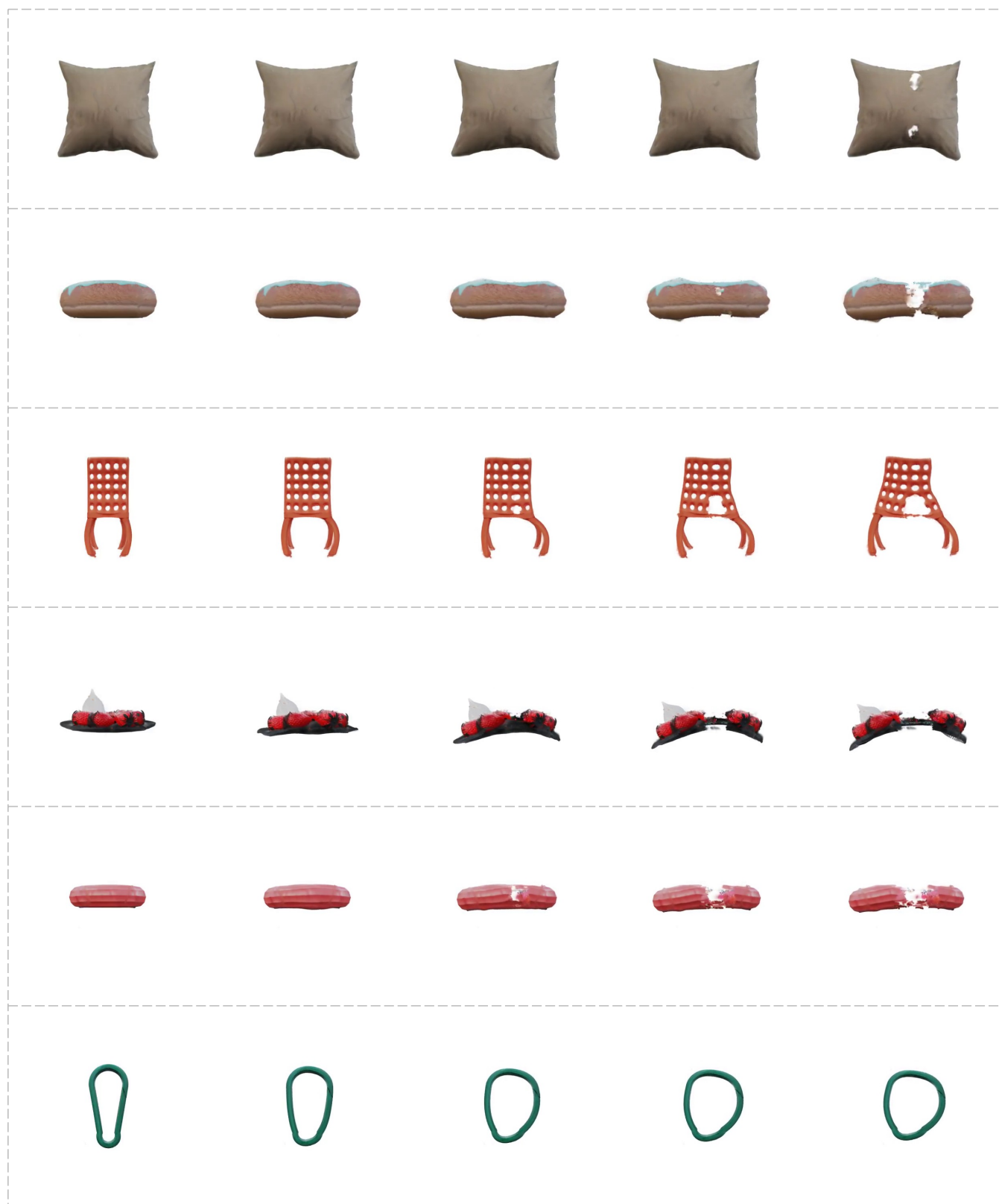


Figure 11: Other results.

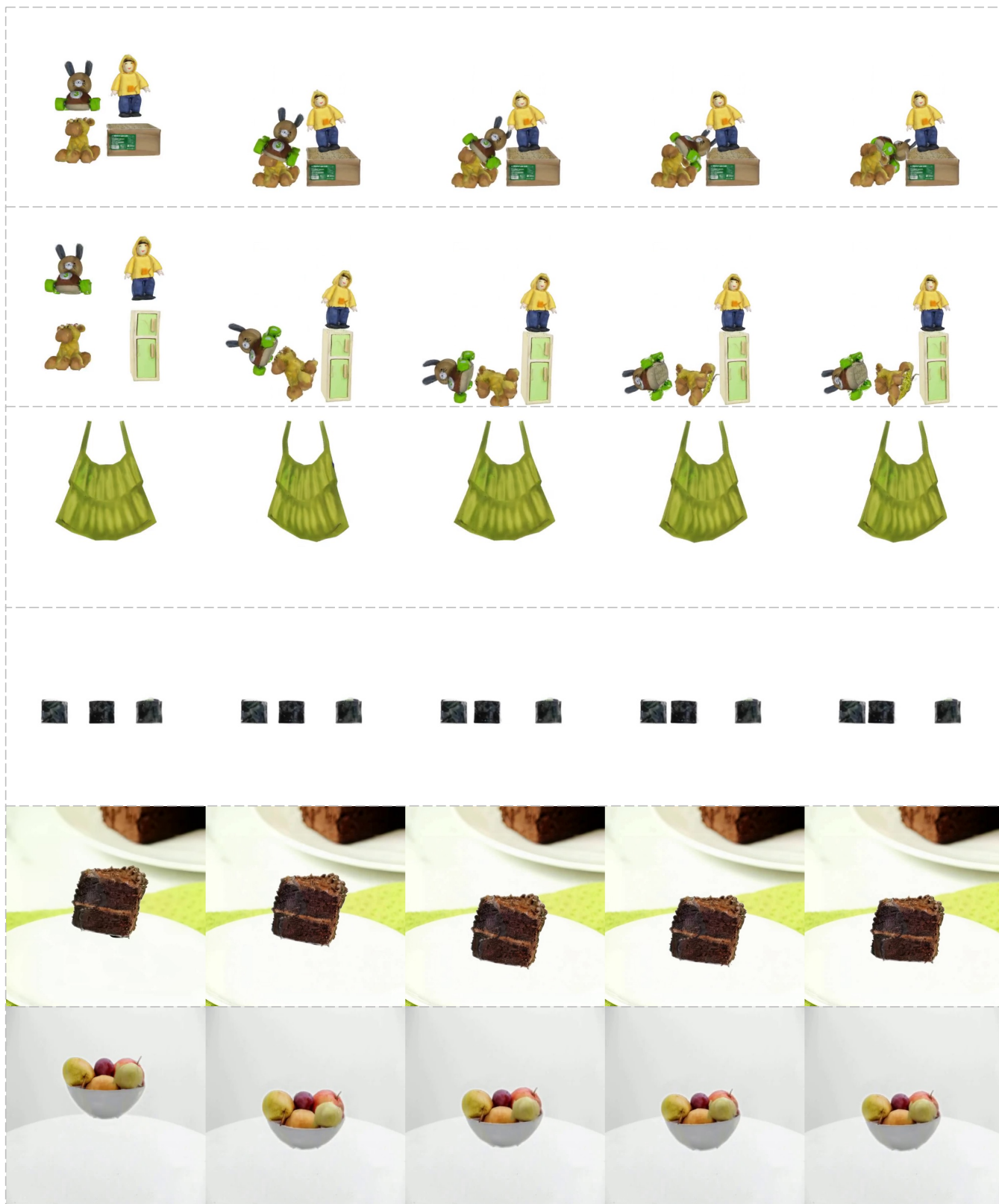


Figure 12: Other results.